Universality and thermoelectric transport properties of quantum dot systems

D. F. Aranguren-Quintero,[1] E. Ramos,[2] J. Silva-Valencia,[1] M. S. Figueira,[3] L. N. Oliveira,[4] and R. Franco[1,*]

[1]*Departamento de Física, Universidad Nacional de Colombia (UNAL), A. A. 5997, Bogotá, Colombia*

[2]*División de Ciencias Básicas, Fundación Universidad de America, Bogotá, Colombia*

[3]*Instituto de Física-Universidade Federal Fluminense (IF-UFF), Avenida Litorânea s/n, CEP:24210-346, Niterói, Rio de Janeiro, Brazil*

[4]*Instituto de Física de São Carlos–Universidade de São Paulo (IFSC-USP), 369 São Carlos, São Paulo, Brazil*

(Received 28 November 2020; revised 16 January 2021; accepted 21 January 2021; published 9 February 2021)

We discuss the temperature-dependent thermoelectric transport properties of semiconductor nanostructures comprising a quantum dot coupled to quantum wires: the thermal dependence of the electrical conductance, thermal conductance, and thermopower. We explore the universality of the thermoelectric properties in the temperature range associated with the Kondo crossover. In this thermal range, general arguments indicate that any equilibrium property's temperature dependence should be a universal function of the ratio $T^* = T/T_K$, where T_K is the Kondo temperature. Considering the particle-hole symmetric, spin-degenerate Anderson model, the zero-bias electrical conductance has already been shown to map linearly onto a universal conductance through a quantum dot embedded or side-coupled to a quantum wire. Employing rigorous renormalization-group arguments, we calculate universal thermoelectric transport coefficients that allow us to extend this result to the thermopower and the thermal conductance. We present numerical renormalization-group results to illustrate the physics in our findings. Applying the universal thermoelectric coefficients to recent experimental results of the electrical conductance and thermovoltages versus V_{gate}, at different temperatures in the Kondo regime, we calculate all the thermoelectric properties and obtain simple analytical fitting functions that can be used to predict the experimental results of these properties. However, we cannot check all of them, due to the lack of available experimental results over a broad temperature range.

DOI: 10.1103/PhysRevB.103.085112

I. INTRODUCTION

The discovery of the Seebeck and Peltier effects in different metal junctions at the beginning of the 19th century gave rise to a branch of physics called "thermoelectric" (TE) [1]. Seebeck observed that when two different metals are joined together (thermocouple) with the junctions maintained at different temperatures, a voltage difference is generated proportional to the temperature variation between the couple's ends. Some time later, Peltier observed that when an electric current flows through the Seebeck device, heat is either absorbed or rejected, depending on the direction of the current along the circuit. Today, the Peltier effect is the basis for many TE refrigeration devices, and the Seebeck effect is the basis for TE power generation devices [2].

Ioffe's prediction in the fifties that doped semiconductors could exhibit relatively large thermoelectric effects [3] had a strong impact on the area of TE materials. It was followed step by step by the discovery that a thermojunction between *p*-type Bi_2Te_3 and bismuth exhibits a maximum temperature difference of 26°C and 40°C between *p*-type and *n*-type Bi_2Te_3 [4]. This compound has dominated the whole field of thermoelectric materials; more specifically, the alloys of Bi_2Te_3 with Sb_2Te_3 for *p*-type and Bi_2Se_3 for *n*-type compounds have the highest ZT [see Eq. (7)] at around room temperature compared to any other known material [5], and up until now, it is the working material for most Peltier cooling devices and Seebeck thermoelectric generators.

Most state-of-the-art TE materials have their dimensionless TE figure of merit, ZT, in the interval $ZT \simeq 1$–2.5 (see Fig. 2 in Ref. [6]), which is well below the Carnot efficiency [7]. However, the advent of nanotechnology opens up new possibilities for increasing ZT, mainly due to the level quantization and the Coulomb interaction, leading to essential changes in the system's thermoelectric properties. Some promising compounds are topological insulators and Weyl and Dirac's semimetals, characterized by nontrivial topological orders. The new characteristic of topological insulators is that, besides the conventional semiconductor bulk band structure, they also exhibit topological surface conduction states. Some of the best TE materials are also three-dimensional topological insulators, such as Bi_2Te_3, Bi_2Se_3, and Sb_2Te_3 [8,9].

Thermoelectric devices must have a $ZT \gtrapprox 3$ in order to attain industrial and household spread; their efficiency has improved over the years, but this was not attained until now [6]. This is the reason why thermoelectric generators or thermoelectric refrigerators are not part of our daily technology. They are used in particular fields like the satellite and aerospace industry, where the advantages of not having movable parts and not requiring maintenance overshadow the low efficiency [6]. One example of this is the radioisotope TE generator [10], a nuclear electric generator that exploits a radioactive atom's natural decay, usually plutonium dioxide $^{238}PuO_2$, converting, via the Seebeck effect, the heat released by the disintegrated atoms into electricity. Furthermore, in

*rfrancop@unal.edu.co

the context of today's climate change, research on new TE materials that improve thermal efficiency is essential as part of our efforts to obtain environmentally clean sources of energy.

In this investigation, we focus on studying the semiconductor single-electron transistor (SET), which is the experimental realization of the single-impurity Anderson model (SIAM) for a finite electronic correlation U. The SIAM was experimentally realized by the Goldhaber-Gordon group [11], with complete control over all of the model's parameters. They measured the electric conductance of a SET and showed its universal character. Recently, interest in studying the thermoelectric properties of the SET has greatly increased and has given rise to several papers that discuss it, both from the theoretical side [12–20] and from the experimental one [21–27]. A useful review can be found in Refs. [1,6,7].

Universal relations for the thermal dependence of the thermodynamic properties, in the Kondo regime, for the SIAM are well known, and a didactic discussion can be found in Hewson's book [28]. Costi *et al*. [13,29] showed that in the Kondo limit of the SIAM, the thermoelectric transport coefficients (TTCs) are only functions of $T^* = (\frac{T}{T_K})$, with the temperature T normalized by the Kondo temperature (T_K). For simplicity, we use $(\frac{T}{T_K})$ only in the figures; in the text, we use T^*. They also showed that by employing the numerical renormalization group (NRG), the electric conductance, the temperature-normalized thermal conductance, and the thermopower exhibit universal behavior in the Kondo regime.

The universal behavior of $G(T^*)$ in semiconductor nanostructures was studied in earlier papers [30,31]. The authors derived an analytical expression that maps the thermal dependence of $G(T^*)$ of a Kondo-asymmetric condition of the SIAM to the universal conductance function $G_S(T^*)$. The corresponding TTC $L_0(T^*)$ [Eq. (27)] was calculated by employing the NRG. This analytical mapping is parametrized by T_K and the ground-state phase shift $\delta = \frac{\pi n_d}{2}$, which is related to Friedel's sum rule [28,32]. For brevity, we call this quantity parameter δ. In this investigation, we derive similar analytical expressions associated with the other TTCs, allowing us to obtain both the thermopower and the thermal conductance in a Kondo-asymmetric situation, employing only universal functions derived from the thermal dependence of the symmetric SIAM. Again, those analytical functions are parametrized by the Kondo temperature and the parameter δ.

In Sec. II, we define the problem and the model employed in the study of the SET. In Sec. III, we define the thermoelectric properties and their relation with the TTCs. In Sec. IV, we develop the calculations of a mapping between the thermal dependence of the TTC coefficients in the symmetric limit and the asymmetric condition in the quantum dot's (QD's) Kondo regime. In Sec. V, we present the results of our research associated with the TTCs and discuss their physical consequences. In Sec. VI, we make a comparison between our results and the available experimental one. In Sec. VII, we present a summary and the conclusions of this investigation. In the Appendix, we develop a methodology to apply universal TTCs to experimental TE properties; we obtain simple analytical fitting functions that can be used to predict these properties' observed behavior.

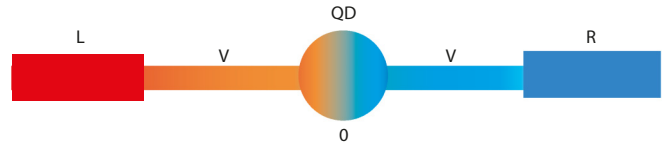

FIG. 1. Schematic of a semiconductor electron transistor (SET): a quantum dot embedded in conduction leads.

II. THE HAMILTONIAN FOR THE SET

In this investigation, we extend the previous results obtained for the electrical conductance $G(T^*)$, associated with the TTC $L_0(T^*)$ [12,13,30], to all the other TTCs: $L_1(T^*)$ and $L_2(T^*)$. We map the thermal dependence of the TTCs for a Kondo-asymmetric situation as a function of the TTCs for a Kondo-symmetric condition. These mappings are obtained in terms of the renormalized Kondo temperature T^* and the parameter δ.

The standard Hamiltonian for the SET studied in this investigation can be written as

$$H = \sum_{\mathbf{k},\sigma}\sum_{\alpha=L,R} E^{\alpha}_{\mathbf{k},\sigma} c^{\alpha\dagger}_{\mathbf{k},\sigma} c^{\alpha}_{\mathbf{k},\sigma} + (E_d n_d + U n_{d\uparrow} n_{d\downarrow}) + \sum_{\alpha=L,R}\sum_{\mathbf{k},\sigma} \frac{V_\alpha}{\sqrt{2N}} \left(c^{\dagger}_{d\sigma} c^{\alpha}_{\mathbf{k},\sigma} + c^{\alpha\dagger}_{\mathbf{k},\sigma} c_{d\sigma}\right), \tag{1}$$

where the first term represents the left ($\alpha = L$) and right ($\alpha = R$) leads, characterized by hot and cold free conduction electron (c-electron) reservoirs, respectively. The quantum dot is embedded in the leads as visually represented in Fig. 1. The second term describes the QD characterized by the local dot energy E_d, and U represents the on-site Coulomb repulsion between the electrons of the QD [33–35]. The third term corresponds to the tunneling between the immersed dot and the left (L) and right (R) semi-infinite leads. The amplitude V_α is responsible for the tunneling between the QD and the lead α. For simplicity, we assume symmetric junctions (i.e., $V_\alpha = V_L = V_R = V$) and identical leads (i.e., $E^L_{\mathbf{k},\sigma} = E^R_{\mathbf{k},\sigma} = E_{\mathbf{k},\sigma}$) connecting the QD to the quantum wire. The $L(R)$ semi-infinite leads comprise N states $c^L_{\mathbf{k},\sigma}$ ($c^R_{\mathbf{k},\sigma}$) with energies defined by the linear dispersion relation $E_{\mathbf{k},\sigma} = (k - k_F)v_F$ ($0 \leqslant k \leqslant 2k_F$) so that the bandwidth is $2D = 2v_F k_F$, with D being the half-width of the conduction band. In all the numerical calculations, we consider the unit of energy to be $D = 1$.

III. THERMOELECTRIC PROPERTIES

We calculated the electrical conductance $G(T)$, the thermal conductance $\kappa_e(T)$, and the thermopower $S(T)$ (Seebeck effect) in terms of the transport coefficients, following the standard textbook derivation [36,37], and the results are

$$G(T) = e^2 L_o(T), \tag{2}$$

$$\kappa_e(T) = \frac{1}{T}\left(L_2(T) - \frac{L_1^2(T)}{L_o(T)}\right), \tag{3}$$

and

$$S = \left(\frac{-1}{eT}\right)\frac{L_1(T)}{L_o(T)}. \tag{4}$$

To calculate the transport coefficients $L_o(T)$, $L_1(T)$, and $L_2(T)$, we employed the results derived by Dong and Lei [38]. They considered the particle current and thermal flux formulas, through an interacting QD connected to the leads at different temperatures, within the Keldysh nonequilibrium Green's function formalism. The electric and thermoelectric transport coefficients were obtained in the presence of the chemical potential and temperature gradients, with the Onsager relation in the linear regime being automatically satisfied. The transport coefficients are given by

$$L_n(T) = \frac{2}{h}\int\left(-\frac{\partial n_F(\omega,T)}{\partial\omega}\right)\omega^n\tau(\omega,T)d\omega, \tag{5}$$

where $n_F(\epsilon,T) = 1/(1+e^{(\epsilon-\mu)/k_BT})$ is the Fermi-Dirac distribution, with μ being the chemical potential, and the transmittance $\tau(\omega,T)$ is given by

$$\tau(\omega,T) = \pi\Gamma\rho_d(\omega,T), \tag{6}$$

where $\rho_d(\omega,T)$ is the spectral density of the QD, $\Gamma = \pi\rho_c(\mu=0)V^2$ is the Anderson parameter, which is a measure of the d-level width, and $\rho_c(\omega) = \frac{1}{2D}$ is the flat conduction density of states of the leads.

A useful quantity that indicates the system performance is the TE dimensionless figure of merit ZT [3], which is given by

$$ZT = \frac{S^2TG}{\kappa_e}. \tag{7}$$

IV. UNIVERSAL MAPPING: TRANSMISSION COEFFICIENT AND THERMOELECTRIC COEFFICIENTS

Following Ref. [30], we introduce the normalized even ($a_{\mathbf{k},\sigma}$) and odd ($b_{\mathbf{k},\sigma}$) operators, in order to exploit the inversion symmetry of the system:

$$a_{\mathbf{k},\sigma} = \frac{1}{\sqrt{2}}\left(c^L_{\mathbf{k},\sigma} + c^R_{\mathbf{k},\sigma}\right), \tag{8}$$

$$b_{\mathbf{k},\sigma} = \frac{1}{\sqrt{2}}\left(c^L_{\mathbf{k},\sigma} - c^R_{\mathbf{k},\sigma}\right). \tag{9}$$

It is convenient to write the Hamiltonian, Eq. (1), on the basis of the new operators ($a_{\mathbf{k},\sigma}$ and $b_{\mathbf{k},\sigma}$), to "split" it into two decoupled pieces $H = H_A + H_B$, with

$$H_A = \sum_{\mathbf{k},\sigma} E_{\mathbf{k},\sigma}a^\dagger_{\mathbf{k},\sigma}a_{\mathbf{k},\sigma} + \sum_\sigma V(f_0^\dagger c_{d,\sigma} + \text{H.c.}) + (E_d n_d + U n_{d\uparrow}n_{d\downarrow}), \tag{10}$$

where $f_0 = \sum_{\mathbf{k},\sigma}(\frac{a_{\mathbf{k},\sigma}}{\sqrt{N}})$ is the traditional NRG shorthand notation, and H_B is given by

$$H_B = \sum_{\mathbf{k},\sigma} E_{\mathbf{k},\sigma}b^\dagger_{\mathbf{k},\sigma}b_{\mathbf{k},\sigma}. \tag{11}$$

The Hamiltonian H_B is quadratic and can be exactly diagonalized and decoupled from the QD. On the contrary, the Hamiltonian H_A "carries" all the correlation effects of the QD and the coupling between it and the conduction band. Due to this, the Hamiltonian H_A is the only one relevant for obtaining the transmittance and the spectral density of states for the quantum dot and can be written as [30]

$$\rho_d(\omega,T) = \frac{1}{f(\omega,T)}\sum_{mn,\sigma}\frac{e^{-\beta E_m}}{Z(T)} \times |\langle n|c^\dagger_{d,\sigma}|m\rangle|^2\delta(E_{mn}-\hbar\omega). \tag{12}$$

Here $|m\rangle$ and $|n\rangle$ are the eigenstates of H_A, with eigenvalues E_m and E_n, respectively, $E_{mn} = E_m - E_n$, and $Z(T)$ is the partition function for Hamiltonian H_A. Hamiltonian H_B is not dependent on $c_{d,\sigma}$, $[H_B, c_{d,\sigma}] = 0$, and only the eigenvalues and eigenvectors of H_A are required to obtain $\rho_d(\omega,T)$. On the other hand, to calculate the matrix elements $\langle n|c^\dagger_{d,\sigma}|m\rangle$ in Eq. (12), we evaluate the commutator $[H_A, a_{\mathbf{q},\sigma}]$,

$$[H_A, a_{\mathbf{q},\sigma}] = E_{q,\sigma}a^\dagger_{\mathbf{q},\sigma} + \frac{V}{\sqrt{N}}c_{d,\sigma}, \tag{13}$$

and performing the summation over q and σ we obtain

$$[H_A, f_0^\dagger] = \frac{1}{\sqrt{3}}f_1^\dagger + Vc_d^\dagger, \tag{14}$$

where

$$f_1 = \sqrt{\frac{3}{N}}\sum_q\left(\frac{E_q}{D}\right)a_q \tag{15}$$

defines a new NRG shorthand notation operator.

Equation (14) permits us to relate the matrix elements $\langle n|c^\dagger_{d,\sigma}|m\rangle$ in Eq. (12) with the same matrix elements of the operators f_0 and f_1,

$$V\langle m|c_d^\dagger|n\rangle = E_{mn}\langle m|f_0^\dagger|n\rangle - \sqrt{3}D\langle m|f_1^\dagger|n\rangle, \tag{16}$$

and a Schrieffer-Wolff transformation of Hamiltonian H_A allows us to write it in the Kondo form [30],

$$H_J = \sum_k E_l g_l^\dagger g_l + J_W\sum_{\mu,\nu}\Phi^\dagger_{0\mu}\sigma_{\mu\nu}\Phi_{0\nu}\cdot\mathbf{S}, \tag{17}$$

where the g_l operators are the eigenoperators of the fixed-point Hamiltonian, associated with the unstable local moment (LM) condition of the Anderson impurity model (see Ref. [30] for details). Here, $J_W = 4D\frac{\Gamma U}{\pi|E_d|(E_d+U)}\cos^2\delta_{\text{LM}}$, where δ_{LM} is the quantum scattering phase shift, associated with the LM fixed point, and

$$\Phi_0 = \frac{1}{\sqrt{N}}\sum_l g_l, \tag{18}$$

where in the symmetric condition $\delta_{\text{LM}} = 0$ and $\Phi_0 = f_0$.

The second term in Eq. (17) is responsible, in the Kondo regime, for the evolution from the LM fixed point to a Fermi liquid fixed point, associated with an antiferromagnetic J_W coupling, characteristic of the Kondo effect. We can define the operator

$$\Phi_1 = \sqrt{\frac{3}{N}}\sum_l\left(\frac{E_l}{D}\right)g_l \tag{19}$$

in a way analogous to the f_1 operator's definition [Eq. (15)]. In the symmetric condition $\Phi_1 = f_1$, and something similar happens with $\Phi_0 = f_0$.

Equations (13) and (16) show the universal character of the product $V\langle m|c_d^\dagger|n\rangle$ at the symmetric point (remember

$\Phi_0 = f_0$ and $\Phi_1 = f_1$ in this condition). In order to explore what happens in the asymmetric condition, it is necessary to relate the operators f_0 and f_1 to Φ_0 and Φ_1 (see Appendix A2 in Ref. [29]). Substituting Eq. (A21) from Ref. [29] in Eq. (16) we obtain

$$\sqrt{\pi\rho\Gamma}\langle m|c_d^\dagger|n\rangle 1 = \alpha_0\langle m|\Phi_0^\dagger|n\rangle + \alpha_1\langle m|\Phi_1^\dagger|n\rangle. \tag{20}$$

Performing the substitution of Eq. (20) in Eq. (12), we obtain the localized QD spectral density $\rho_d(\omega, T)$, which can be written as

$$\pi\rho\Gamma\rho_d(\omega, T) = \alpha_0^2\rho_0(\omega, T) + \alpha_1^2\rho_1(\omega, T) + \alpha_0\alpha_1\rho_{(01)}(\omega, T), \tag{21}$$

where $\rho_0(\omega, T)$, $\rho_1(\omega, T)$, and $\rho_{(01)}(\omega, T)$ are universal expressions of the Kondo regime and are given by

$$\rho_j(\omega, T) = \sum_{mn} \frac{e^{-\beta E_m}}{Z(T)f(\omega, T)}|\langle n|\Phi_j|m\rangle|^2 \times\delta(E_{mn} - \hbar\omega) \quad (j = 0, 1) \tag{22}$$

and

$$\rho_{(01)}(\omega, T) = \sum_{mn} \frac{e^{-\beta E_m}}{Z(T)f(\omega, T)}(\langle n|\Phi_0|m\rangle \times\langle n|\Phi_1|m\rangle + \text{c.c.})\delta(E_{mn} - \hbar\omega). \tag{23}$$

Substituting Eq. (21) in Eq. (6), the transmittance at energy $\epsilon = \frac{\hbar\omega}{2\pi}$ and temperature T is given by

$$\tau(\omega, T) = \frac{\alpha_0^2}{\rho}\rho_0(\omega, T) + +\frac{\alpha_1^2}{\rho}\rho_1(\omega, T) + \frac{\alpha_0\alpha_1}{\rho}\rho_{(01)}(\omega, T). \tag{24}$$

The universal expressions $\rho_0(\omega, T)$, $\rho_1(\omega, T)$, and $\rho_{(01)}(\omega, T)$ "carry" the thermal dependence of $\tau(\omega, T)$. The important point that should be stressed here is that the transmittance is the key physical quantity that enters the calculations of all the TE coefficients given by Eq. (5). All the dependence of the parameters of the model is taken into account through the coefficients α_0 and α_1, given by the reference [30]

$$\alpha_0^2 = \cos^2(\delta), \tag{25}$$

$$\alpha_1^2 = \frac{6}{\pi^2}\sin^2(\delta). \tag{26}$$

Taking into account the result of Eqs. (5) and (24), it is possible to compute the thermal dependence of the linear TTCs as a function of (T^*),

$$L_0(T^*) - \frac{1}{h} = -\left(L_0^S(T^*) - \frac{1}{h}\right)\cos(2\delta), \tag{27}$$

where $L_0^S(T^*)$ is the universal coefficient L_0 in the electron-hole symmetric condition of the model, when $E_d = \frac{-U}{2}$ and $\delta = \frac{\pi n_d}{2}$, with $n_d = 1$. All the thermal dependence of $L_0(T^*)$ is contained in the universal function $L_0^S(T^*)$. The function $\cos(2\delta)$ carries all the parameter dependence apart from temperature T and is characteristic of the asymmetric conditions for the model ($\delta \neq \frac{\pi}{2}$).

Taking into account that $\mathcal{G}_2(T) = e^2L_0(T)$, we can write Eq. (27) in the same form as a result obtained in Ref. [30],

$$G_2(T^*) - \mathcal{G}_2 = -\left(\mathcal{G}_2^S(T^*) - \mathcal{G}_2\right)\cos(2\delta), \tag{28}$$

where we also should observe that the $\rho_{(01)}(\omega, T)$ term in Eq. (24), due to particle-hole symmetry arguments, makes no contribution to the TE coefficients L_0 [39] and L_2 but contributes to L_1, as indicated in Eqs. (29) and (30).

The evaluation of the L_1 coefficient, employing the result for the transmission coefficient [Eq. (24)] in Eq. (5) ($n = 1$) and taking into account the parity condition of the integrand give us

$$L_1(T^*) = L_{(01)}(T^*)\cos(\delta)\sin(\delta), \tag{29}$$

where

$$L_{(01)}(T) = \frac{\sqrt{2}\pi}{h\rho}\int_{-D}^{D}\epsilon\rho_{(01)}(\epsilon, T)\left(-\frac{\partial f(\epsilon, T)}{\partial\epsilon}\right)d\epsilon, \tag{30}$$

which is a universal function of (T^*) in the symmetric Kondo condition and contains all the thermal dependence of $L_1(T^*)$.

Finally, employing the result for the transmittance [Eq. (24)] in Eq. (5) ($n = 2$), we obtain the $L_2(T^*)$ coefficient. Again, we take into account the parity of the integrand,

$$\frac{L_2(T^*)}{\left(\frac{k_BT}{T_K}\right)^2} - \frac{\pi^2}{6} = -\cos(2\delta)\left(\frac{L_2^S(T^*)}{\left(\frac{k_BT}{T_K}\right)^2} - \frac{\pi^2}{6}\right). \tag{31}$$

The quantity $\frac{L_2^S(T^*)}{\left(\frac{k_BT}{T_k}\right)^2}$ is a universal function of (T^*), obtained in terms of $L_2^S(T)$, the coefficient for the symmetric condition of the model. As in the previous cases, all the thermal dependence of Eq. (31) in any asymmetric condition of the model is contained in $\frac{L_2^S(T^*)}{\left(\frac{k_BT}{T_K}\right)^2}$, and all the dependence on the parameters of the model is taken into account through the scattering phase shift factor δ.

V. RESULTS AND DISCUSSION: UNIVERSAL MAPPING

In previous papers [30,31,39,40] one of us (L.N.O.) argued that it is possible to employ experimental data on electrical conductance $G(T^*)$ to obtain the parameter δ and, with it, "check" the validity of Eq. (27) for the SET. Computations for the case of a side-coupled QD were also considered in Refs. [31,39,40], including a comparison with experimental results [39]. In all those previous papers, the numerical calculations were done employing the NRG, including computation of the parameter δ.

The NRG logarithmic discretization parameter employed in the simulations in this work was $\Lambda = 2.25$ and the chemical potential, $\mu = 0.0D$. The Kondo temperature, T_K, in each case was obtained by computing the value of the temperature, where the electrical conductance attains the value $G(T_K) = \frac{G_o}{2} = \frac{e^2}{h}$ [41].

Figure 2 shows the results obtained for the electrical conductance $G(T)$ vs T^*, in units of $G_o = \frac{2e^2}{h}$, in an asymmetric situation employing the results of the symmetrical limit as shown in Fig. 11 in the Appendix. We plot results corresponding to the Kondo regime, employing the parameters $E_f = -5.0D$ and $U = 30.0D$, with the Kondo temperature

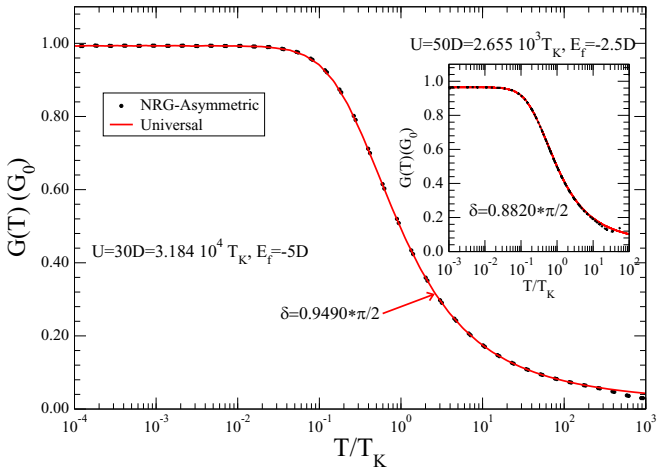

FIG. 2. The electrical conductance $G(T)$ vs T^*, corresponding to the Kondo regime. Inset: Another situation, closer to the crossover between the Kondo and the intermediate valence regime.

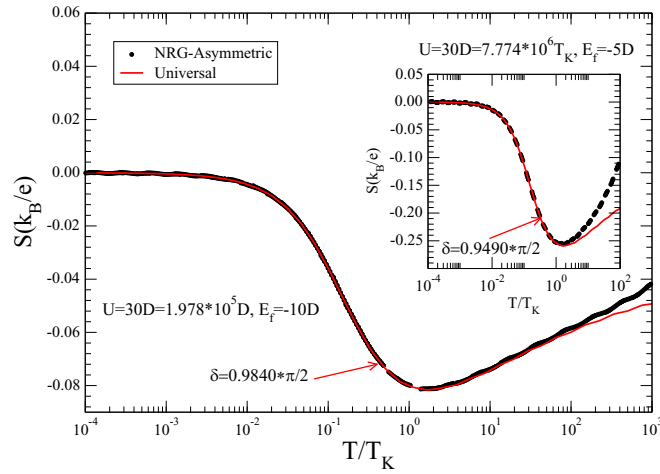

FIG. 4. Thermopower $S(T^*)$ in $\frac{K_B}{e}$ units vs T^*. Inset: The crossover's results from the intermediate valence to the Kondo regime.

being $T_K = 9.422.10^{-4}D$. The agreement between the calculated NRG asymmetric results and those obtained employing the NRG symmetric one, Eq. (27), is notable. The parameter δ computed by the NRG for the asymmetric case is $\delta = 0.9490\frac{\pi}{2}$, which confirms the validity of Eq. (27) for the SET, previously obtained in Ref. [30]. In the inset in Fig. 2, we plot a situation closer to the crossover transition between the Kondo and the intermediate valence regime, with $U = 50.0D$, $E_f = -2.5D$, $T_K = 1.883 \times 10^{-2}D$, and $\delta = 0.882\frac{\pi}{2}$. The agreement obtained is notable for temperatures below $T \simeq 10T_K$, but for temperatures above this value, the results show a small departure from each other, due to the rising of charge fluctuations not being well described by the present treatment.

In Fig. 3 we show the results for $(\frac{L_1}{T})$ vs T^* for the asymmetric Kondo limit, with $E_{\rm QD} = -10.0D$, $U = 30.0D$, and $T_K = 1.517 \times 10^{-5}D$. The direct NRG computations are shown by the solid red line, whereas the results obtained when employing the NRG calculations for the particle-hole symmetric case of the SIAM and Eq. (29) are shown by the black curve. Again, the parameter δ was computed following the procedure described in the Appendix. We obtained an excellent agreement for a large range of temperatures, $10^{-4}T_K \leqslant T \leqslant 10^3T_K$. In the inset in Fig. 3, we show the same results, but now for a set of parameters closer to the crossover transition region, between the Kondo and the intermediate valence regimes, with $E_{\rm QD} = -5.0D$, $U = 30.0D$, and $T_K = 9.422 \times 10^{-4}D$.

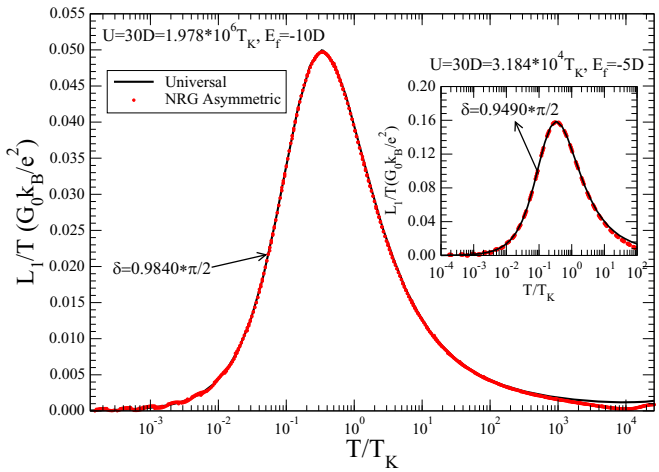

FIG. 3. Universal thermoelectric coefficient $(\frac{L_1}{T})$, expressed in $\frac{G_o k_B}{e^2}$ units, vs T^* for the asymmetric Kondo limit. Inset: The same results for an asymmetric case, in the crossover from an intermediate valence situation to the Kondo limit.

In Fig. 4, we plot the thermopower $S(T^*)$ vs T^* for $E_{\rm QD} = -10.0D$, $U = 30.0D$, and $T_K = 1.517 \times 10^{-5}D$. Employing Eqs. (4), (27), and (29) (red curve), we obtain an excellent agreement between the asymmetric direct NRG results (black curve) and those employing the symmetric universal TTCs. The minimum at the Kondo temperature manifests the Kondo effect on the thermopower $S(T)$ [13]. There is excellent agreement between both curves up to $T \leqslant 10^2T_K$, when charge fluctuations dominate the process. In the inset in Fig. 4, we represent a crossover from the intermediate valence to the Kondo regime $E_{\rm QD} = -5.0D$, $U = 30.0D$, and $T_K = 9.422 \times 10^{-4}D$. Below $T \geqslant T_K$, the agreement between the two curves is excellent, but above T_K, there is a visible difference between the two results at higher temperatures. We attribute this difference to the intermediate valence region's proximity, because the present treatment does not describe charge fluctuations well.

In Fig. 5, we plot the results for the universal thermoelectric coefficient for the asymmetric Kondo limit, $(\frac{L_2}{T^2})$ vs T^* in G_oL_N units, where $L_N = (\frac{\pi^2}{3})(\frac{k_B}{e})^2$ is the Lorenz number, with $E_{\rm QD} = -5.0D$, $U = 30.0D$, and $T_K = 9.422 \times 10^{-4}D$. Again, the agreement obtained between the direct asymmetric NRG results and those obtained employing Eq. (31) and particle-hole symmetric NRG results (fitting presented in Fig. 13) is excellent. In the inset in Fig. 5, we show the temperature-normalized electronic contribution to the thermal conductance $(\frac{\kappa}{T})$ vs T^*. In this case, some small differences appear above $T \geqslant 30.0T_K$, which is a manifestation of the

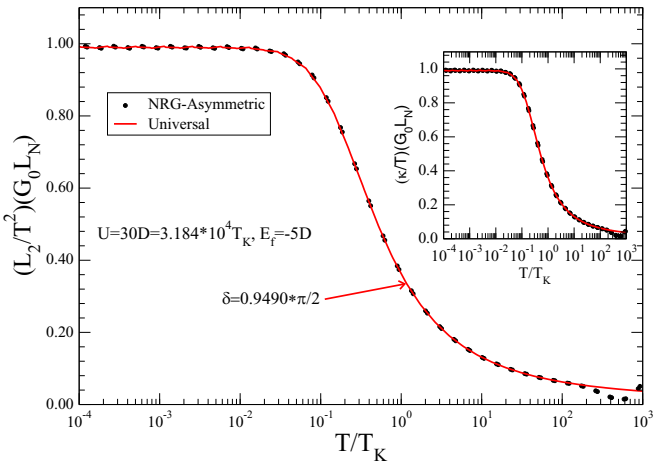

FIG. 5. Universal thermoelectric coefficient ($\frac{L_2}{T^2}$), in G_oL_N units, vs T^* for the asymmetric Kondo limit. Inset: Temperature-normalized electronic contribution to the thermal conductance ($\frac{\kappa}{T}$) vs T^*.

charge fluctuation process, present in this range of temperatures.

Figure 6 shows the thermal dependence of the universal quantities in the symmetric limit of the SIAM, employing the parameters $U = 30.0D$, $E_f = -15.0D$. We plot the temperature-normalized electronic contribution to the thermal conductance ($\frac{\kappa(T)}{T}$) and the electric conductance $G(T)$ vs T^*. The striking similarity of both curves at low temperatures is associated with the Fermi liquid character of the system and the validity of the Wiedemann-Franz law in this temperature range [12,13], which leads to the relation $\frac{\kappa(T)}{T} = G(T)$. However, besides the relative closeness of the curves well below and above the Kondo temperature, the two properties are not equal once the Kondo temperature rules the electrical conductance, whereas the thermal conductance is ruled by a

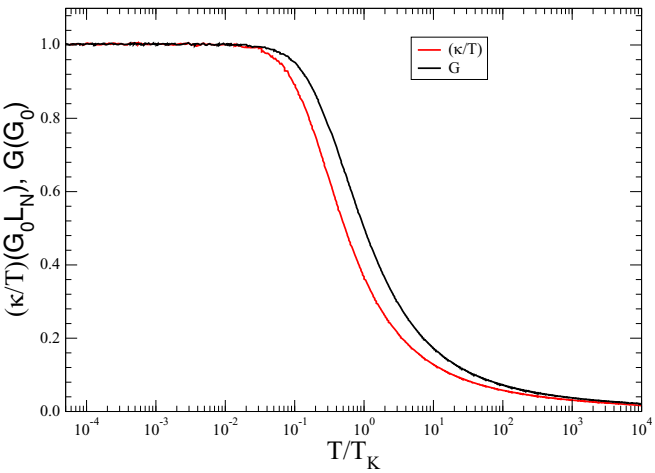

FIG. 6. Thermal dependence of universal quantities in the symmetric limit. Temperature-normalized electronic contribution to the thermal conductance $\kappa(T)/T$ and the electric conductance $G(T)$ vs T^*.

different Kondo scale T_K^θ, as defined in Ref. [13],

$$\frac{\kappa\left(T = T_K^\theta\right)}{T_K^\theta} = \frac{\tilde{\alpha}}{2}, \tag{32}$$

where

$$\tilde{\alpha} = \lim_{T\to 0} \frac{\kappa(T)}{T}. \tag{33}$$

VI. COMPARISON WITH EXPERIMENTAL RESULTS

In this section, we discuss how to use the methodology employing the universal TTCs to calculate the TE properties from experimental measurements. In the Appendix, we present a discussion and some examples of applying the universal TTC methodology to experimental thermoelectric data.

Unfortunately, we did not find experimental SET works in the literature that performed measurements of the electric and thermal conductances and the thermopower in a broad range of temperatures. On the other hand, several papers measured the gate dependence $V_{\text{gate}} = V$ of some of these properties for a fixed temperature, T [23,25,27,42,43]. We focus on applying the universal TTC methodology to the experimental results of the Svilans *et al*. paper [25], because they performed several high-quality TE measurements of Kondo correlated QDs, both below and above the Kondo temperature. They measured the electric conductance $G(T)$, thermocurrent I_{Th} normalized by ΔT (under closed-circuit conditions), and thermovoltage V_{th} (under open-circuit conditions) as a function of the gate voltage V for a fixed temperature.

Considering an ohmic dependence between the thermovoltage and the thermocurrent in an experimental device, the relation $SG = \alpha \frac{I_{\text{Th}}}{\Delta T}$ is valid, where ΔT is the difference in temperatures associated with the Seebeck effect and where α must be a dimensionless constant for a fixed V_{gate}, but it can be a temperature function. If we assume that at low temperatures $\alpha = \eta T$, with η being a constant that has the

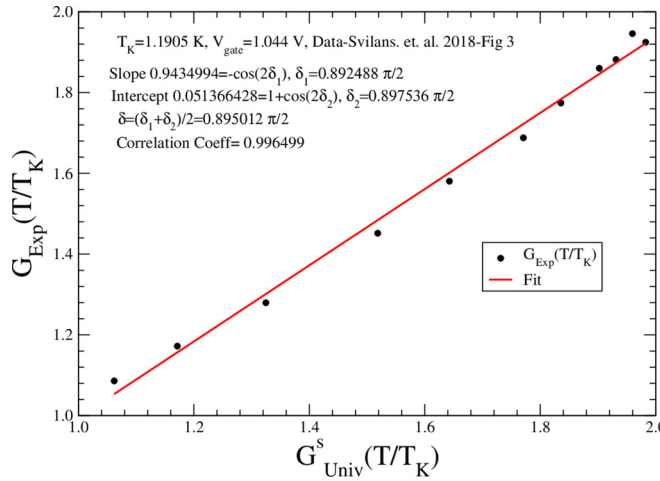

FIG. 7. $G(T^*)$ vs $G^S(T^*)$, where experimental data were obtained from the Svilans *et al*. experimental paper [25] with $V_{\text{gate}} = 1.044$ V [see Eq. (28)].

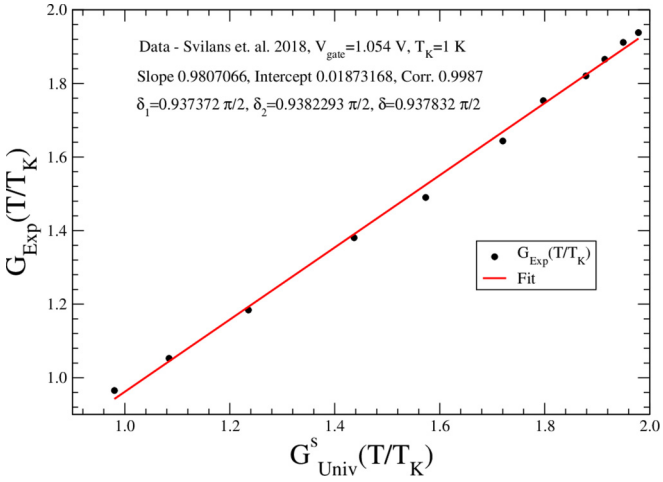

FIG. 8. $G(T^*)$ vs $G^S(T^*)$, where experimental data were obtained from the Svilans *et al*. experimental paper [25] with $V_{\text{gate}} = 1.054$ V [see Eq. (28)].

inverse of temperature units, we expected that

$$\frac{I_{\text{Th}}}{\Delta T} \simeq \frac{SG}{T}. \tag{34}$$

To explore the validity of our predictions, we employed the following results from the Svilans *et al*. paper [25]: the data from Figs. 2(b), 3(a) and 3(b), for the electrical conductance $G(T)$ at different gate voltages V_{gate}, and Figs. 2(c) and 4(a), which present the results for $\frac{I_{\text{Th}}}{\Delta T}$ as a function of V_{gate} at different temperatures.

In Figs. 7 and 8, we show the results for the slope and the intercept of the linear figures corresponding to the electrical conductance $G(T)$ of the Svilans *et al*. [25] experimental data. We obtained $\delta = 0.895\,012\pi/2$ and $T_K = 1.1905$ K for $V_{\text{gate}} = 1.044$ V and $\delta = 0.937\,832\pi/2$ and $T_K = 1.0$ K for $V_{\text{gate}} = 1.054$ V. These Kondo temperatures agree well with the experimental results indicated in Fig. 3(b) of Ref. [25].

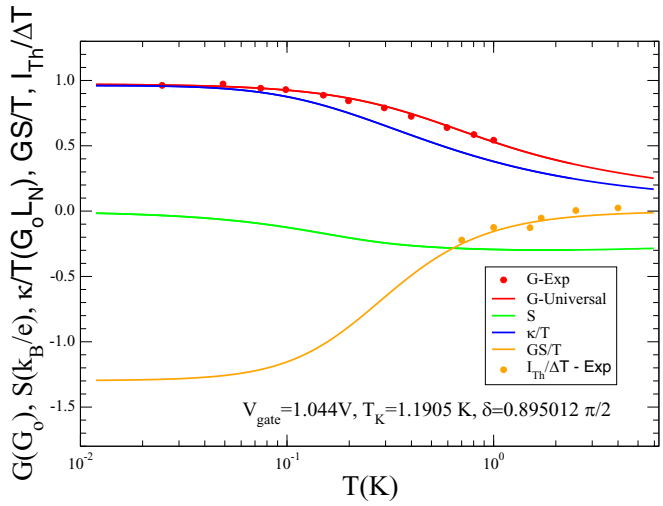

FIG. 9. Thermoelectric properties as a function of the temperature in degrees kelvin. Experimental data were obtained from the Svilans *et al*. experimental paper [25] with $V_{\text{gate}} = 1.044$ V.

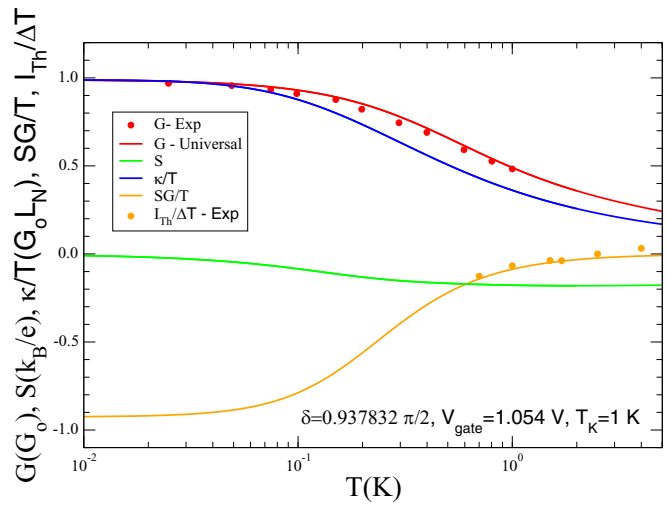

FIG. 10. Thermoelectric properties as a function of the temperature in degrees kelvin. Experimental data were obtained from the Svilans *et al*. experimental paper [25] with $V_{\text{gate}} = 1.054$ V.

Employing the δ and T_K values obtained, the universal relations for the Onsager coefficients [Eqs. (27)–(31)], and Eqs. (2)–(4), we compute the thermal dependence of the TE properties: $G(T)$, $S(T)$, $\frac{\kappa}{T}$, and GS/T. In Fig. 9, we show the results of these properties, corresponding to $V_{\text{gate}} = 1.044$ V. Initially, we adjust the universal electrical conductance $G_{\text{Universal}}$ to the corresponding experimental one, $G -$ Exp., and we compute $\frac{SG}{T}$ and compare it with the experimental data on $\frac{I_{\text{Th}}}{\Delta T}$. Unfortunately, the number of experimental data for the $\frac{I_{\text{Th}}}{\Delta T}$ in the Svilans *et al*. paper is limited, but the agreement of both properties with the available experimental data is excellent. Although there are no available experimental results for the temperature-normalized thermal conductance κ/T or the thermopower $S(T)$, we calculated these properties and obtained fair, reliable results: κ/T exhibits behavior similar to that in Fig. 6, and $S(t)$ goes to 0 at low temperatures, indicating that the experimental measurements were performed in a Kondo situation nearer the symmetric limit.

In Fig. 10, we show the same results as in Fig. 9, corresponding to $V_{\text{gate}} = 1.054$ V, and the results show the same overall behavior as the previous ones.

VII. CONCLUSIONS

In the present investigation, we employ the NRG treatment to compute the thermal dependence of the TTCs in the Kondo regime. From Eqs. (27)–(31), we can obtain the thermal dependence of the thermoelectric transport coefficients L_0, L_1, and L_2 under asymmetric conditions in terms of the Kondo temperature and the parameter δ. All of the thermal dependence is "carried" through the symmetric TE coefficients' universal functions of T^*, and all of the dependence on the parameters of the model is taken into account through the parameter δ. We also derived simple universal fitting formulas for the TTCs, given by Eqs. (A3), (A4), and (A5), discussed in the Appendix, which can be used to predict the TE properties.

In practical terms, knowledge of the experimental results of the electrical conductance or the thermopower in the Kondo

regime at temperature function $\{G(T_i), T_i\}$ or $\{S(T_i, T_i\}$ allows the determination of the Kondo temperature T_K and the parameter δ, and employing the TTCs, we can calculate all the other thermoelectric properties.

The ideal situation to "check" our procedure is to obtain all the TE properties from the experimental measurements, but this requires a consistent and complete set of experimental data for $G(T)$, $S(T)$, and $\kappa(T)$, over a broad temperature range below and above the Kondo temperature, for the same V_{gate}. Unfortunately, we did not find such experimental measurements in the literature, but several papers have measured the gate dependence $V_{\text{gate}} = V$ of these properties for a fixed temperature, T [23,25,27,42,43].

We focused on applying the universal TTC methodology to the experimental results of the Svilans *et al*. paper [25], which measured the electric conductance $G(T)$, thermocurrent I_{Th} normalized by ΔT, and thermovoltage V_{th} as a function of the gate voltage V for a fixed temperature. We adjusted the experimental results for $G(T)$ and $I_{\text{Th}}/\Delta T$ employing the universal TTCs, obtaining excellent agreement. Although the Svilans group did not measure the temperature-normalized thermal conductance κ/T or the thermopower $S(T)$, we calculated these properties, obtaining reliable results.

We expect that this investigation will motivate researchers to carry out experimental work in this direction, in order to compare the procedure expounded here to experimental testing.

ACKNOWLEDGMENTS

We are thankful for the financial support of the Research Division of the Colombia National University, Bogotá (DIB); the Colombian Scientific Agency COLCIENCIAS; the São Paulo State Research Foundation (FAPESP); the Brazilian National Research Council (CNPq); and the Coordination of Superior Level Staff Improvement (CAPES). E.R. acknowledges support from COLCIENCIAS-COLFUTURO doctoral scholarship Convocatoria Doctorados Nacionales No. 617, 2014-2. R.F. is grateful for the hospitality of IFSC-USP-São Carlos and IF-UFF-Niterói, where part of this work was done.

APPENDIX: APPLICATION OF THE UNIVERSAL TTC METHODOLOGY TO EXPERIMENTAL DATA

Some earlier papers [30,31,39,40] have discussed how to employ experimental data on the thermal dependence of the electric conductance $G(T)$ to calculate the parameter δ to check the validity of Eq. (27). In particular, an almost-perfect fit of $G(T)$ with experimental results was found in Ref. [44]. From the theoretical point of view, it is possible to adjust the experimental results by employing the TTCs in the symmetrical limit of the SIAM obtained from the NRG calculations. Nevertheless, for practical purposes, we can also employ the fitting formulas obtained in Eqs. (A3), (A4), and (A5).

Essentially, the procedure is the following: Given a set of experimental data $[G_i(T_i), T_i]$, choose a trial Kondo temperature T_K and a new data set, $[G_i(T_i^*), T_i^*]$ with $T_i^* = \frac{T_i}{T_K}$, is generated. Since the universal curve for the electric conductance in the symmetric limit of the SIAM, $G^S(T^*)$ vs T^*, is known for the fitting of Eq. (A3) (Fig. 11), it is possible to obtain the value $G_i^S(T_i^*)$ for each experimental data set of T_i^* and plot $G_i(T_i^*)$ vs $G_i^S(T_i^*)$. If the plot follows a straight line, the correct Kondo temperature value T_K is attained, and the corresponding parameter δ can be obtained from the slope and the intercept of the straight line [see Eq. (28) and Figs. 7 and 8]. On the contrary, if the obtained plot does not follow a straight line, a new trial Kondo temperature T_K must be employed, until a straight line is obtained. Employing Eq. (27) and the fit shown in Eq. (A3), it is also possible to compute $L_0(T^*)$.

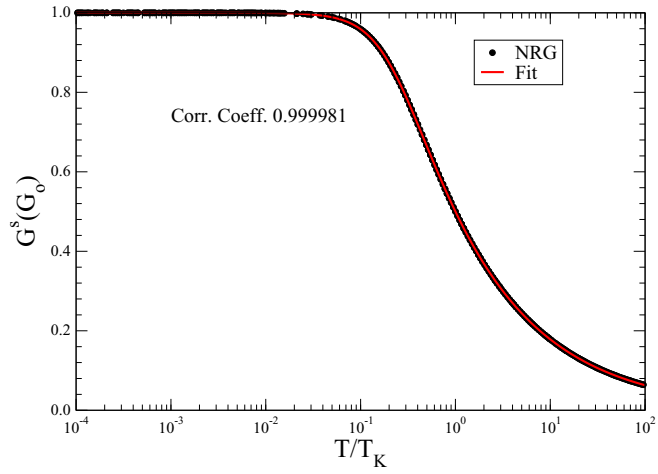

FIG. 11. NRG universal electrical conductance $G^S(G_o)$ in the symmetrical limit of the SIAM vs (T^*) and its fit to Eq. (A3).

The same procedure can be performed using the thermopower. Employing Eqs. (4), (27), and (29), it is possible to write the thermopower S as

$$\frac{e}{h}S(T^*) = \frac{\sin(2\delta)\left(\frac{L_{01}^S}{T}\right)(T^*)}{-4\cos^2(\delta) + 2h\cos(2\delta)L_0^S(T^*)}, \tag{A1}$$

which is equivalent to the equation

$$\frac{h}{e}\frac{\left(\frac{L_{01}^S}{T}\right)(T^*)}{S(T^*)} = -2\cot(\delta) + 2h\cot(2\delta)L_0^S(T^*). \tag{A2}$$

Given a set of temperatures and a thermopower experimental data set T_i and $S(T_i)$ $(i = 1, \ldots, N)$ $([S(T_i), T_i])$, we can choose a tentative Kondo temperature T_K, compute T_i^*, and obtain $[S_i(T_i^*), T_i^*]$. Since we know the universal functions $L_0^S(T_i^*)$ [fitting of $G_0^S(T_i^*)$, Eq. (A3), associated with Fig. 11] and $\frac{L_{01}^S}{T}(T_i^*)$, it is then a simple matter to compute the fraction on the left-hand side and plot it as a function of $L_0^S(T_i^*)$. If the plot is a straight line, the Kondo temperature has been found. If not, we continue the process until the correct value is attained.

Once the correct parameters δ and T_K are obtained, it is possible to compute $\frac{L_1}{T}(T^*)$ employing the universal function $\frac{L_{(10)}}{T}(T^*)$ given by Eq. (29) or the adjusted Eq. (A4) of the results shown in Fig. 12. Additionally, it is possible to compute the quantity $\frac{L_2(T^*)}{(k_B T^*)^2}$ by employing Eq. (31) or the fit [Eq. (A5)] of the results shown in Fig. 13. Finally, using Eqs. (2)– (4), we can calculate $G(T^*)$, $S(T^*)$, and $\kappa(T^*)$ and, with these, other quantities, such as ZT and the Wiedemann-Franz law.

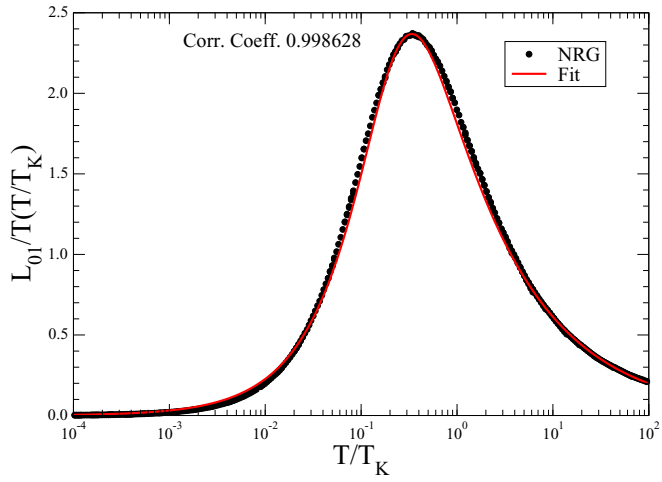

FIG. 12. Thermal dependence of the universal function $(\frac{L_{(01)}}{T})$ vs T^*, in the symmetric limit of the SIAM, and its fit to Eq. (A4).

In Fig. 11, we plot the NRG universal result [29] for the electrical conductance in the symmetrical limit of the Kondo regime $G^S(T^*)$, employing the following parameters: $U = 30.0D$ and $E_f = -15.0D$. The red line is the fit of the NRG data using a one-parameter equation employed in Ref. [41],

$$G(T^*) = \frac{Go}{[(T^*)^2(2^{1/\xi} - 1) + 1]^{\xi}}, \tag{A3}$$

to adjust the electrical conductance. The parameter ξ determines the steepness of the decrease in conductance with increasing temperature and provides a good fit to the NRG results for the Kondo regime. In our case, $\xi = 0.226\,022$ and the correlation coefficient equals 0.999 986. The agreement achieved is excellent. Equation (A3), associated with this fit, allows us to compute the universal TTC $L_0^S(T^*)$ for any T^* value in the range of temperatures presented.

In Fig. 12, we show the thermal dependence of the universal function $(\frac{L_{(01)}}{T})(T^*)$ vs T^* in the symmetric limit of the SIAM, employing the following parameters: $U = 30.0D$ and $E_f = -15.0D$. We obtain a good agreement with the universal

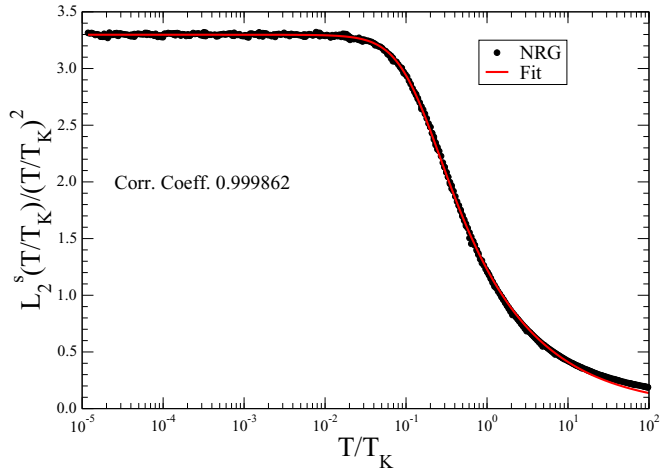

FIG. 13. The universal quantity $\frac{L_2^S(T^*)}{(\frac{k_B T}{T_K})^2}$ vs T^*, obtained by the NRG, and its fit to Eq. (A5).

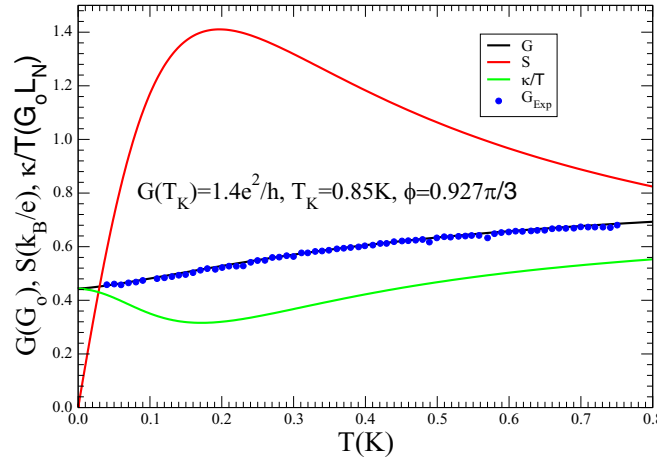

FIG. 14. Electrical and thermal conductances and thermopower vs temperature (in kelvins) for a side-coupled SET, obtained from the experimental electrical conductance at $T_K = 0.85$ K [45].

TTC $(\frac{L_{(01)}}{T})(T^*)$ (red line), employing a three-parameter fit expression similar to Eq. (A3),

$$\left(\frac{L_{(01)}}{T}\right)(T^*) = A_0\left(\frac{(T^*)^{\frac{A_1}{\xi}}}{(T^*)^2\left[A_2^{1/\xi} - 1\right] + 1}\right)^{\xi}, \tag{A4}$$

where $A_0 = 11.945\,007$, $A_1 = 0.860\,404$, $A_2 = 63.2865$, and $\xi = 0.674\,506$.

In Fig. 13, we plot the NRG universal results obtained for the TTC $\frac{L_2^S(T^*)}{(k_B T^*)^2}$ in the symmetric limit of the SIAM, employing the following parameters: $U = 30.0D$ and $E_f = -15.0D$. The red line is the fit of the NRG numerical data to Eq. (A5); the agreement achieved is excellent. Again, the expression associated with this fit has a form similar to that of Eq. (A3),

$$\frac{L_2^S}{(T^*)^2} = \frac{A_0}{[(T^*)^2(2^{1/\xi} + A_1) + 1]^{\xi}}, \tag{A5}$$

where $A_0 = 3.297\,76$, $\xi = 0.238\,365$, and $A_1 = 43.6995$. This formula reduces to Eq. (A3) if $A_0 = G_0$ and $A_1 = -1.0$.

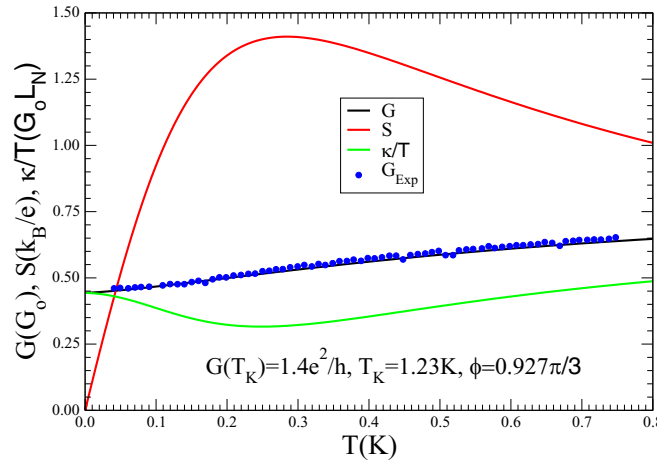

FIG. 15. Electrical and thermal conductances and thermopower vs temperature (kelvins) for a side-coupled SET, obtained from the experimental electrical conductance at $T_K = 1.23$ K [45].

It also permits computation of $\frac{L_2^S(T^*)}{(k_B T^*)^2}$ for any T^* value in the temperature range indicated in Fig. 13.

For completeness, we also repeat earlier calculations employed in [39], which obtained the electrical conductance and the Kondo temperature using the experimental results of the electrical conductance SET in a side-coupled geometry [45]. We show the results of those calculations in Figs. 14 and 15. The fit of the electrical conductance is excellent. We also calculate $S(T)$ and $\kappa(T)/T$, but we cannot check the reliability of these results, due to the absence of experimental measurements.

[1] D. Sánchez and R. López, C. R. Phys. **17**, 1060 (2016).

[2] T. Tritt, in *Encyclopedia of Materials: Science and Technology*, edited by K. J. Buschow, R. W. Cahn, M. C. Flemings, B. Ilschner, E. J. Kramer, S. Mahajan, and P. Veyssiere (Elsevier, Oxford, UK, 2002), p. 1.

[3] A. F. Joffe and L. S. Stil, Rep. Prog. Phys. **22**, 167 (1959).

[4] D. A. Wright, Nature **181**, 834 (1958).

[5] I. T. Witting, T. C. Chasapis, F. Ricci, M. Peters, N. A. Heinz, G. Hautier, and G. J. Snyder, Adv. Electron. Mater. **5**, 1800904 (2019).

[6] J. He and T. M. Tritt, Science **357**, eaak9997 (2017).

[7] G. Benenti, G. Casati, K. Saito, and R. Whitney, Phys. Rep. **694**, 1 (2017).

[8] N. Xu, Y. Xu, and J. Zhu, npj Quantum Mater. **2**, 51 (2017).

[9] J. Gooth, G. Schierning, C. Felser, and K. Nielsch, MRS Bull. **43**, 187 (2018).

[10] M. Zoui, S. Bentouba, J. G. Stocholm, and M. A. Bourouis, Energies **13**, 3606 (2020).

[11] D. Goldhaber-Gordon, H. Shtrikman, D. Mahalu, D. Abusch-Magder, U. Meirav, and M. A. Kastner, Nature **391**, 156 (1998).

[12] M. Yoshida and L. Oliveira, Phys. B: Condens. Matter **404**, 3312 (2009).

[13] T. A. Costi and V. Zlatic, Phys. Rev. B **81**, 235127 (2010).

[14] S. Hershfield, K. A. Muttalib, and B. J. Nartowt, Phys. Rev. B **88**, 085426 (2013).

[15] S. Donsa, S. Andergassen, and K. Held, Phys. Rev. B **89**, 125103 (2014).

[16] V. Talbo, J. Saint-Martin, S. Retailleau, and P. Dollfus, Sci. Rep. **7**, 14783 (2017).

[17] T. A. Costi, Phys. Rev. B **100**, 161106(R) (2019).

[18] T. A. Costi, Phys. Rev. B **100**, 155126 (2019).

[19] Y. Kleeorin, H. Thierschmann, H. Buhmann, A. Georges, L. W. Molenkamp, and Y. Meir, Nat. Commun. **10**, 5801 (2019).

[20] U. Eckern and K. I. Wysokiński, New J. Phys. **22**, 013045 (2020).

[21] J. P. Heremans, C. M. Thrush, and D. T. Morelli, Phys. Rev. B **70**, 115334 (2004).

[22] R. Scheibner, E. G. Novik, T. Borzenko, M. König, D. Reuter, A. D. Wieck, H. Buhmann, and L. W. Molenkamp, Phys. Rev. B **75**, 041301(R) (2007).

[23] E. A. Hoffmann, H. A. Nilsson, J. E. Matthews, N. Nakpathomkun, A. I. Persson, L. Samuelson, and H. Linke, Nano Lett. **9**, 779 (2009).

[24] N. Hartman, C. Olsen, S. Lüscher, M. Samani, S. Fallahi, G. C. Gardner, M. Manfra, and J. Folk, Nat. Phys. **14**, 1083 (2018).

[25] A. Svilans, M. Josefsson, A. M. Burke, S. Fahlvik, C. Thelander, H. Linke, and M. Leijnse, Phys. Rev. Lett. **121**, 206801 (2018).

[26] B. Dutta, J. T. Peltonen, D. S. Antonenko, M. Meschke, M. A. Skvortsov, B. Kubala, J. König, C. B. Winkelmann, H. Courtois, and J. P. Pekola, Phys. Rev. Lett. **119**, 077701 (2017).

[27] B. Dutta, D. Majidi, A. García Corral, P. A. Erdman, S. Florens, T. A. Costi, H. Courtois, and C. B. Winkelmann, Nano Lett. **19**, 506 (2019).

[28] A. C. Hewson, *The Kondo Problem to Heavy Fermions* (Cambridge University Press, Cambridge, UK, 1993).

[29] T. A. Costi, A. C. Hewson, and V. Zlatic, J. Phys.: Condens. Matter **6**, 2519 (1994).

[30] M. Yoshida, A. C. Seridonio, and L. N. Oliveira, Phys. Rev. B **80**, 235317 (2009).

[31] A. C. Seridonio, M. Yoshida, and L. N. Oliveira, Phys. Rev. B **80**, 235318 (2009).

[32] D. C. Langreth, Phys. Rev. **150**, 516 (1966).

[33] M. Grobis, I. G. Rau, R. M. Potok, H. Shtrikman, and D. Goldhaber-Gordon, Phys. Rev. Lett. **100**, 246601 (2008).

[34] A. V. Kretinin, H. Shtrikman, D. Goldhaber-Gordon, M. Hanl, A. Weichselbaum, J. von Delft, T. Costi, and D. Mahalu, Phys. Rev. B **84**, 245316 (2011).

[35] J. J. Parks, A. R. Champagne, T. A. Costi, W. W. Shum, A. N. Pasupathy, E. Neuscamman, S. Flores-Torres, P. S. Cornaglia, A. A. Aligia, C. A. Balseiro, G. K.-L. Chan, H. D. Abruña, and D. C. Ralph, Science **328**, 1370 (2010).

[36] G. D. Mahan, *Many-Particle Physics* (Springer-Verlag, Berlin, 1990), p. 227.

[37] J. M. Ziman, *Principles of the Theory of Solids* (Cambridge University Press, Cambridge, UK, 1999), p. 229.

[38] B. Dong and X. L. Lei, J. Phys.: Condens. Matter **14**, 11747 (2002).

[39] A. C. Seridonio, M. Yoshida, and L. N. Oliveira, Europhys. Lett. **86**, 67006 (2009).

[40] L. N. Oliveira, M. Yoshida, and A. C. Seridonio, J. Phys.: Conf. Ser. **200**, 052020 (2010).

[41] D. Goldhaber-Gordon, J. Göres, M. A. Kastner, H. Shtrikman, D. Mahalu, and U. Meirav, Phys. Rev. Lett. **81**, 5225 (1998).

[42] R. Scheibner, H. Buhmann, D. Reuter, M. N. Kiselev, and L. W. Molenkamp, Phys. Rev. Lett. **95**, 176602 (2005).

[43] S. F. Svensson, E. A. Hoffmann, N. Nakpathomkun, P. M. Wu, H. Q. Xu, H. A. Nilsson, D. Sánchez, V. Kashcheyevs, and H. Linke, New J. Phys. **15**, 105011 (2013).

[44] L. Merker, S. Kirchner, E. Muñoz, and T. A. Costi, Phys. Rev. B **87**, 165132 (2013).

[45] M. Sato, H. Aikawa, K. Kobayashi, S. Katsumoto, and Y. Iye, Phys. Rev. Lett. **95**, 066801 (2005).